Chapter 2

The Antiresonant Reflecting Optical Waveguide Fiber Sensor

Ran Gao and Jiansen Ye

Abstract

In this chapter, the optical fiber sensors based on antiresonant reflecting optical waveguide have been introduced, including the single layer, double layers, double resonators, and hybrid mechanism. Various optical fiber sensors based on antiresonant reflecting optical waveguide have been introduced in this chapter with different working principles, including the fiber optic vibration sensor, humidity sensor, strain sensor, temperature sensor, magnetic field sensor, biosensor, etc. Especially, many long-standing challenges in the fiber optic sensor can be solved through the working principle of the antiresonant reflecting optical waveguide, including the temperature cross-talk compensation, distribution localization, optofluidic biosensing, etc. In general, the optical fiber sensors based on antiresonant reflecting optical waveguide have advantages, such as compact structure, high sensitivity, large dynamic range, and high stability, which appear to have potential applications in researches of structure health monitoring, oil exploiting, and biology detection.

Keywords: antiresonant reflecting optical waveguide, Fabry-Pérot resonator, double layers, double resonators, hybrid mechanism

1. Background

Over past two decades, the antiresonant reflecting optical waveguide (ARROW) has developed into a versatile platform for a range of interdisciplinary applications in low loss communication [1], ultrafast optics [2], optical amplifiers [3], and biophotonics [4]. In the ARROW, the guided light is reflected at the two surfaces of the cladding in the hollow-core fiber (HCF), forming a Fabry-Pérot etalon [5]. The guided light at the antiresonant wavelength can be propagated along the HCF. Due to the unique light guiding mechanism, the ARROW is a good candidate for the fiber optic sensor: (i) the optical properties of the ARROW can be easily manipulated with the cladding structure, making the flexibility for fiber optic sensors; (ii) the guided light can break the confining of the fiber core, forming an enhanced interaction between the light and the ambient medium; and (iii) the hollow holes in the HCF is a natural channel for the optofluidic biosensors, which reduce the complexity of the fiber optic sensor significantly. Many sensing principles of ARROWs for fiber optic sensors have been researched in recent years, including the ARROW with the single layer, double layers, double resonators, hybrid mechanism, etc. [6]. The ARROW-based fiber optic sensors possess great flexibility, high sensitivity, and low cost, which are expected to be used for many fields in real-world

Sensors	Performance	Application
Vibration sensor	(1) Signal-to-noise ratio of 60 dB, (2) wide frequency response from 5 to 10 kHz, and (3) high sensitivity and low temperature cross-sensitivity	Applications for the monitoring of smart structures such as buildings, bridges, highways, pavements, dams, and so on
Humidity sensor	(1) The sensitivity of up to 0.22 dB/% RH and (2) good repeatability, fast response time, and low temperature cross-sensitivity	Applications for human daily biology, industrial production, agriculture, animal husbandry, and other fields
Water-level sensor	Sensitivity of 1.1 dB/mm	Applications for water-level monitoring
Strain sensor	(1) The resolution of the sensor is 27.9 pm/με and (2) the temperature cross-sensitivity is only 1.67 pm/°C	Applications for the accurate measurement of the strain of smart structures
Magnetic field sensor	(1) Magnetic field sensitivity of 81 pm/Oe and (2) low temperature cross-sensitivity	Applications for industrial production, motor, and electronic products' magnetic field measurement
Optic biosensors	(1) The limit of detection of 0.5 ng/ml can be achieved for the IFN-γ concentration and (2) the influence of the temperature could be compensated through the referenced resonance dip	Applications for health monitoring, cancer prevention, biological engineering, etc.
Pressure sensor	(1) The pressure sensitivity of −4.42 nm/MPa and (2) the spatial sensitivity of 0.86 nm/cm can be achieved	Applications for multipoint pressure detection in the fields of security, structure monitoring, and oil exploration
Temperature sensor	Temperature sensitivity of 70.71 pm/°C	Applications for biomedicine, industrial production, space exploration, and other fields

Table 1.
The optical fiber sensor based on ARROW [7–15].

applications [5, 6]. The optical fiber sensor based on the principle of ARROW is mainly applied in the optical fiber vibration sensor, optical fiber humidity sensor, water-level sensor, fiber strain sensor, fiber optic magnetic field sensor, fiber optic biosensors, optical fiber pressure sensor, optical fiber temperature sensor, and other types of optical fiber sensors. The common optical fiber sensors based on the ARROW principle and their performance are shown in **Table 1**.

2. The principle of the antiresonant reflecting optical waveguide

The antiresonance reflection principle refers to light that does not meet the resonance condition and is confined to the low refractive index (RI) fiber core for transmission [5]. In 1986, the antiresonant reflecting optical waveguide (ARROW) was proposed by Duguya et al. [5]. The working principle of the ARROW is to use the design of the multilayer high reflection film between the waveguide and silicon substrate (most of which use the double-layer film) to transmit the light beam in the waveguide layer, so as to reduce the energy leakage, with the characteristics of single mode and small loss [5, 6, 16]. The ARROW structure is a promising waveguide structure for silicon-based sensors and has been used for a variety of purposes because it allows the thickness of the buffer layer to be reduced and the single-mode size to be increased and the process tolerance and material selection range to be relatively expanded [17–19].

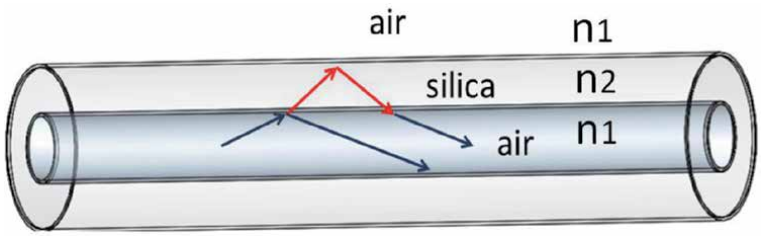

Figure 1.
The structure of ARROW.

The ARROW can be used to study the optical conduction mechanism of low-index core fibers, which is similar to Fabry-Pérot resonators [6]. **Figure 1** shows the structure diagram of the ARROW, where the gray part is the high-index layer with RI n2 (silica) corresponding to the Fabry-Pérot resonator cavity and the dark gray part is the low-index layer with RI n1 (air) [17, 18]. When the wavelength of the optical fiber satisfies the resonance condition, it will leak out from the high fold rate layer corresponding to the low transmission intensity part of the transmission spectrum, which is similar to the destructive interference of light in the Fabry-Pérot cavity [19, 20]. In contrast, the light of the antiresonance wavelength will be reflected back at the interface of the high and low RIs and will be restricted to be transmitted in the fiber core. So most of the light will be reflected back to the fiber core [20]. Based on the principle of the antiresonant waveguide, the optical fiber sensor can be made into different types by changing the relevant parameters. Optical fiber sensors based on the antiresonant waveguide are mainly divided into two types [21]. The first is to change the resonant wavelength by changing the RI or the length of the Fabry-Pérot cavity. The second is to change the contrast of the output intensity of the antiresonant waveguide by changing the associated external material composition [19, 20]. The optical fiber sensor of the ARROW finally realizes the measurement of different physical quantities through these two kinds of modulation methods. This chapter will introduce the working principles of various ARROW-based fiber optic sensors in detail [20, 21].

3. The antiresonant reflecting optical waveguide sensor

3.1 The single-layered antiresonant reflecting optical waveguide sensor

The simplest model of the antiresonant reflecting optical waveguide (ARROW) is the single-layered antiresonant reflecting optical waveguide (SL-ARROW), which is widely used in optical fiber sensors. The SL-ARROW mode in the capillary waveguide is sensitive to the surrounding environments, and various sensing applications have been proposed, such as vibration sensor, humidity sensor, water-level sensing, etc. The working principle of the SL-ARROW is introduced by the vibration sensor [7].

Vibration signal detection is very important in the application of structural monitoring in people's life. Vibration detection can monitor the safety of building structures such as buildings, highways, bridges, dams, highways, and so on. In general, the vibration can be detected by piezoelectric, magneto-electric, and current sensors [22]. SL-ARROW is an optical fiber vibration sensor, which is designed based on the principle of antiresonant waveguide. The fiber optic sensor is a good alternative with several unique advantages such as low weight, immunity to electromagnetic interference, and long-distance signal transmission for remote

operation [23]. Here, an all-fiber vibration sensor based on the SL-ARROW has been proposed in a tapered capillary fiber. The schematic construction of the proposed vibration sensor is given in **Figure 2**. In order to fabricate the sensor, the capillary optical fiber is selected as the sensing fiber. The capillary fiber consists of a hollow core with an inner diameter of 30 μm and a ring-cladding with a thickness of 55 μm. Both ends of the 8 cm long capillary optical fiber are cut by the high-precision cutter, and the cut capillary fiber and single-mode fiber (SMF) are spliced through the fiber splicer. The cross section of the capillary fiber and the splicing diagram between the capillary fiber and SMF are shown in **Figure 2** [7].

The principle of using capillary fiber to make vibration sensor can be described as an SL-ARROW [24]. As the RI of the cladding is larger than that of the core, the core mode can oscillate and radiate through the cladding. The cladding modes propagate in the cladding region of the capillary fiber, as shown in **Figure 3(a)**. The working principle of the tapered capillary fiber can be approximated to Fabry-Pérot etalon, as shown in **Figure 3(b)**. When the wavelengths cannot satisfy the resonant condition, the optical waveguide will be confined in the hollow core of the fiber as the core modes. Therefore, the guide light can be reflected by the resonator. On the contrary, when the wavelength meets the resonant condition, the guided light will resonate and will not be reflected by the Fabry-Pérot cavity and will leak out of the

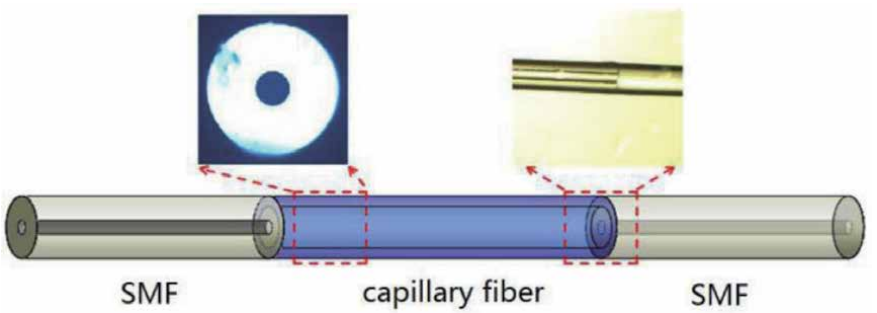

Figure 2.
The schematic construction of the proposed sensor [7].

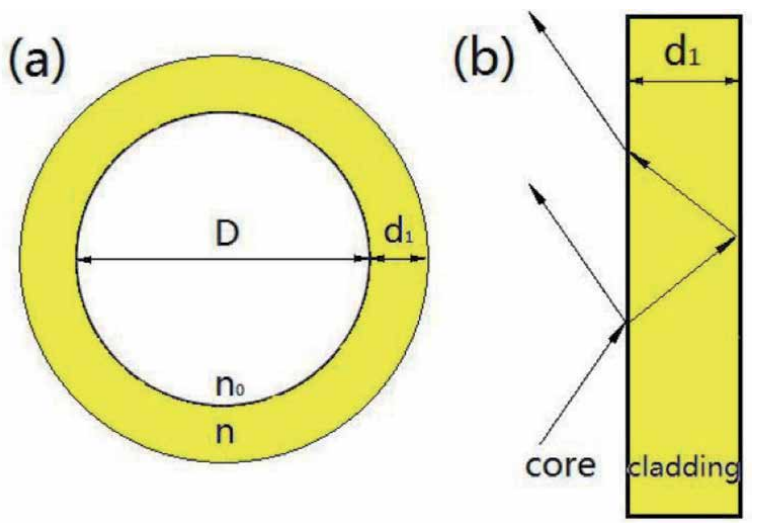

Figure 3.
(a) Schematic diagram of the cross section of the capillary fiber and (b) the guiding mechanism of the capillary fiber [7].

cladding to generate the transmission spectrum. In the transmission spectrum, periodic and narrow loss attenuation corresponding to the Fabry-Pérot cavity resonance condition will appear [7]. The wavelength of the lossy dip corresponding to the resonance condition λ_r can be expressed as Eq. (1) [7, 22]:

$$\lambda_r = \frac{2d\sqrt{n^2 - n_0^2}}{m} \tag{1}$$

where n and n_0 are the RIs of the capillary fiber cladding and air, respectively, d is the thickness of capillary fiber cladding, and m is the resonance order [7].

The mechanical analysis of the photoelastic effect of the tapered region under bending can be expressed as follows [7]:

$$\Delta n = \frac{1}{4}n^2(1+\gamma)(P_{12} - P_{11})\left(\frac{A}{R}\right)^2 \tag{2}$$

where Δn is the change of the RI, n is the RI of the silica, P_{11} and P_{12} are the optoelastic constants of silica, γ is the Poisson ratio of silica, A is the diameter of the tapered region, and R is the bending radius. Substitution of Eq. (1) into Eq. (2) gives

$$\lambda_r = \frac{2(d\sqrt{\left(n + \frac{1}{4}n^2(1+\gamma)(P_{12} - P_{11})\left(\frac{A}{R}\right)^2\right)^2 - n_0^2}}{m} \tag{3}$$

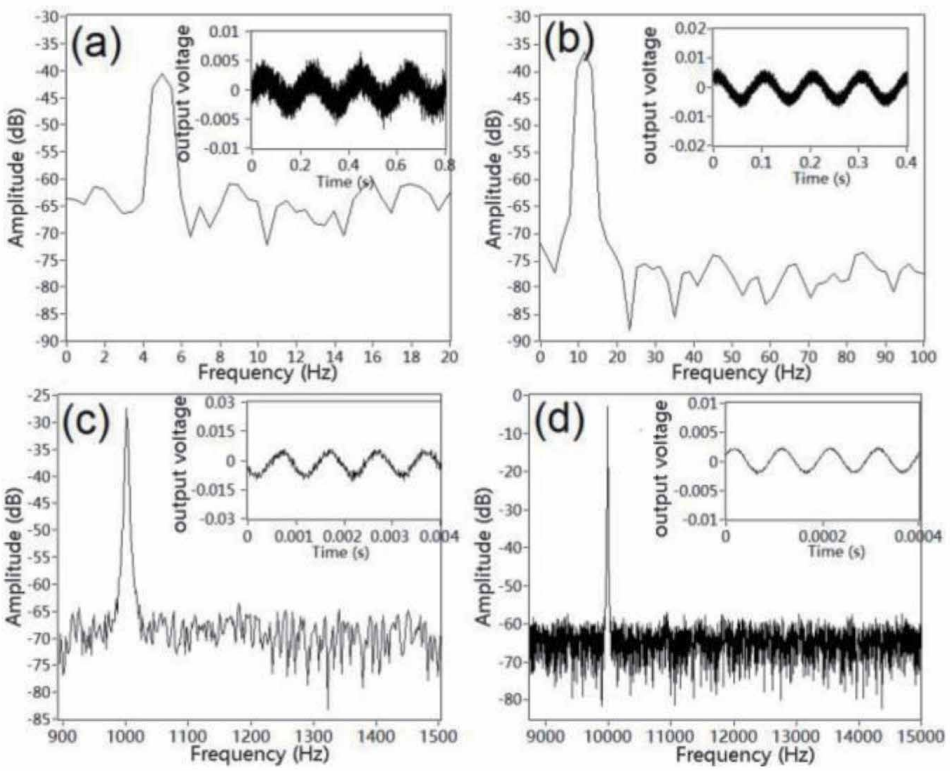

Figure 4.
The frequency spectrum of the tapered capillary fiber corresponding to (a) 5 Hz, (b) 10 Hz, (c) 1 kHz, and (d) 10 kHz [25].

According to Eq. (3), it can be seen that the wavelength of the loss dip in the transmission spectrum under resonance condition is highly sensitive to the small change of bending radius in the tapered region. This provides an attractive method for vibration detection.

To test the frequency response of the fiber vibration sensor, the corresponding frequency response experiments were performed, and the transmission spectra are shown in **Figure 4** [7]. In the fiber vibration sensor experiment, the piezoelectric plate was used as the vibration source, which was driven by 1.8 V sinusoidal signals of 5.0 Hz, 10.0 Hz, 1.0 kHz, and 10.0 kHz, respectively. The transmission intensity of the fiber sensor was converted into a frequency spectrum by fast Fourier transform (FFT), as shown in **Figure 4(a)–(d)** [7]. The corresponding time domain signals are shown in the insets. The sampling rate of each frequency is 1 M and the total sampling time is 5 s. All of transmission intensities of sensor were modulated to sinusoidal waveforms with very uniform amplitude [7]. The main peaks of the frequency spectrum are located at 4.98, 9.98, 998.03, and 9998.96 Hz, respectively, which are close to the corresponding driving frequency [25].

3.2 The double-layered antiresonant reflecting optical waveguide

Compared with the SL-ARROW, the Fabry-Pérot resonator in the ARROW can be also formed through two layers with different claddings of the fiber. A double-layered Fabry-Pérot resonator can be formed between the silica cladding and polymethyl methacrylate (PMMA) cladding [9, 10]. The DL-ARROW possesses high flexibility, which can be used in various sensing applications such as strain sensor, film sensing, temperature, vibration sensing, etc. Taking the temperature sensor as an example, the working principle of the double-layered ARROW (DL-ARROW) is introduced [9].

In real life, optical fiber temperature sensor has been widely used in temperature measurement in different application areas. Optical fiber temperature sensor has many unique advantages such as immunity to electromagnetic interferences, high sensitivity, repeatability, stability, durability, high resolution and fast response, durability against harsh environments, and other advantages [26]. A temperature sensor based on the DL-ARROW was presented [9]. The cross-sectional view of the fiber is given in **Figure 5 (a)**. A section of the simplified hollow-core (SHC) photonic crystal fiber (PCF) was cleaved at both ends, and one end of the fiber was sealed with glue, as can be seen in **Figure 5(b)**, the selectively opened air hole can be seen in **Figure 5(c)**, and the schematic construction of the proposed device is given in **Figure 5(d)** [9].

The essence of the optical fiber temperature sensor guidance is mainly driven by the silicon rod around the hollow core, which plays the role of the ARROW [25]. Before the fiber is penetrated by alcohol, due to the weak interaction between the core and the cladding mode, light is well restricted in the air core of the SHC-PCF. This can be interpreted as a strong lateral field mismatch between the modes, resulting in the overlap with the core field distribution being washed away. **Figure 6** gives the sketch of the optical path of the beams at the alcohol-filled area and the outer silica cladding [9].

In the presence of alcohol in the SHC-PCF cavity, due to the better phase matching, the interaction between the core layer and the cladding mode can be greatly enhanced, resulting in the degradation of the optical field constraints in the hollow core. The core mode field will radiate through the silicone ring around the air core to the outer cladding. The alcohol-filled cavity combined with the external silicon cladding can be regarded as a double-layer Fabry-Pérot resonant cavity

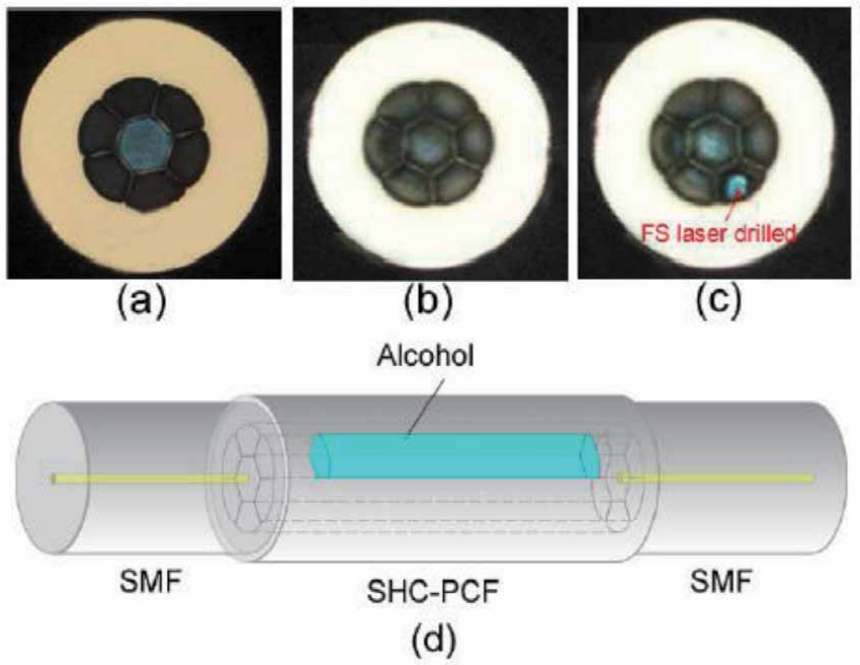

Figure 5.
(a) The cross-sectional view of the SHC-PCF, (b) the SHC-PCF sealed at the end face, (c) with end face sealed selectively opened, and (d) the structure diagram of the sensor.

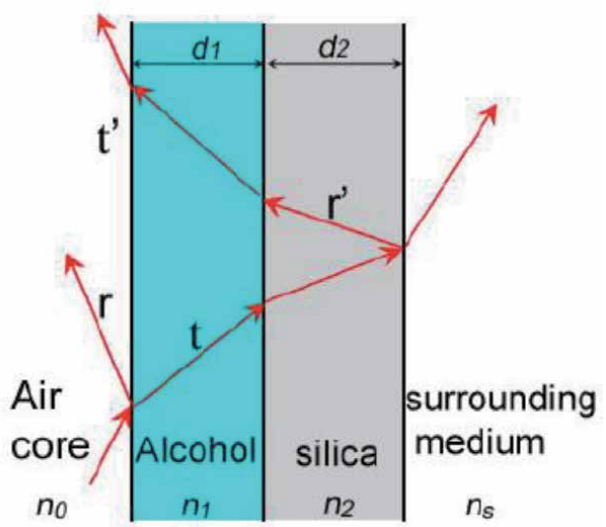

Figure 6.
The optical path of the interference beams at the alcohol-filled area and the outer cladding [10].

[9, 27]. For wavelengths that satisfy the resonance conditions of the resonator, constructive interference occurs, which means that the Fabry-Pérot resonator is highly transparent to these wavelengths, and light cannot be reflected and will leak out of the cladding [27]. In contrast, for the antiresonance wavelength (i.e., the

wavelength that does not satisfy the resonance condition), destructive interference occurs, and light can be well reflected by the Fabry-Pérot resonator [9]. The Fabry-Pérot resonator is confined within the cavity of the optical fiber and serves as a guide for the waveguide mold. The position of the non-transmitted wavelength can be described by the following formula as Eq. (4) [9, 27]:

$$\lambda_m = \frac{2(d_1\sqrt{n_1^2 - n_0^2} + d_2\sqrt{n^2{}_2 - n_0^2}}{m} \tag{4}$$

where d_1 is the thickness of the air cladding, d_2 is the thickness of the outer cladding, and m is a positive integer. n_0, n_1 and n_2 are the refractive indices of air, alcohol and silica, respectively. From Eq. (4), it can be seen that the resonant wavelengths are mainly determined by the thickness of the alcohol and the outer silicon cladding and the material index.

By differentiating Eq. (4) with respect to temperature (T), we get the temperature sensitivity as in Eq. (5). It should be noted that in Eq. (5), we only considered the change of n_1 ($dn_1 = \alpha dT$, α is the thermo-optic coefficient of alcohol), since silica has a much smaller thermo-optic coefficient than alcohol, which can be ignored in this case as Eq. (5) [9]:

$$\frac{\partial \lambda_m}{\partial T} = \frac{2d_1 n_1}{m\sqrt{n_1^2 - n_0^2}}\alpha \tag{5}$$

The thermo-optic coefficient of alcohol is -3.99×10^{-4}.

The temperature response characteristics of this temperature sensor were investigated in a temperature box with adjustable temperature. The temperature sensor with a filling length of 1.2 cm is put into a temperature box. The temperature of the temperature box was heated from room temperature to 60° with an increment of 10°C. The maximum value of temperature measurement is limited below the boiling point of alcohol (78.37°) [9]. This situation can be improved by using a liquid with higher boiling point like ethylene glycol [9]. The attenuation dips were found to shift toward shorter wavelengths with temperature increasing, as can be seen in **Figure 7(a)** [9]. The wavelength shift versus temperature in the experiment is plotted in **Figure 7(b)**, and the temperature sensitivity was obtained to be −0.48 nm/°. [9].

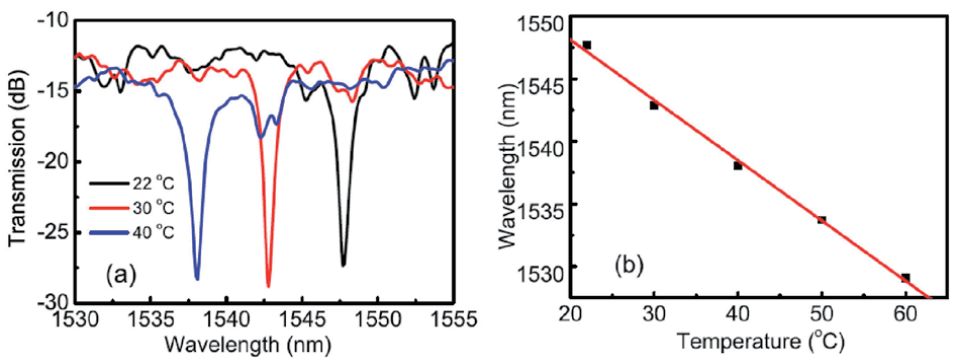

Figure 7.
(a) Spectrum blueshift with increasing of temperature and (b) temperature response of the SHC-PCF with filling length of 2 cm [9].

3.3 The double resonator antiresonant reflecting optical waveguide sensor

Both the SL-ARROW and DL-ARROW are formed to generate the ARROW effect in the fiber optic sensor. However, many long-standing challenges still exist in the ARROW-based fiber sensor, such as serious temperature cross-sensitivity [12]. The ambient temperature change can also modulate the resonance condition of ARROW, making a decrease of the measurement accuracy for both SL-ARROW and DL-ARROW. Therefore, the double resonator ARROW (DR-ARROW) has been investigated to solve the temperature cross talk in the fiber sensor. In this section, the biosensor fiber sensors are taken as examples, and the working principle of the DR-ARROW is introduced [12].

The in-line fiber optofluidic waveguide biosensors possess both enhanced sensing performance and ultracompact size, which have been widely used in the lab-in-fibers chemical and biological sensing [12]. In-line fiber biosensors possess many distinctive advantages such as high sensitivity, compact size, and immunity to electromagnetic interference [28]. Here, a biosensor based on DR-ARROW for the detection of interferon-gamma (IFN-γ) concentration has been introduced. The schematic construction of the proposed biosensor sensor is given in **Figure 8**. In the proposed sensor, a HCF was employed as the sensing fiber, as shown in **Figure 8(a)**. The HCF consists of an air octagon core, an air-ring cladding with eight holes, and a silica cladding. The NaCl solution was filled into a cladding hole with a length of 10 cm through the capillary force by immersing the remaining SMF into the NaCl

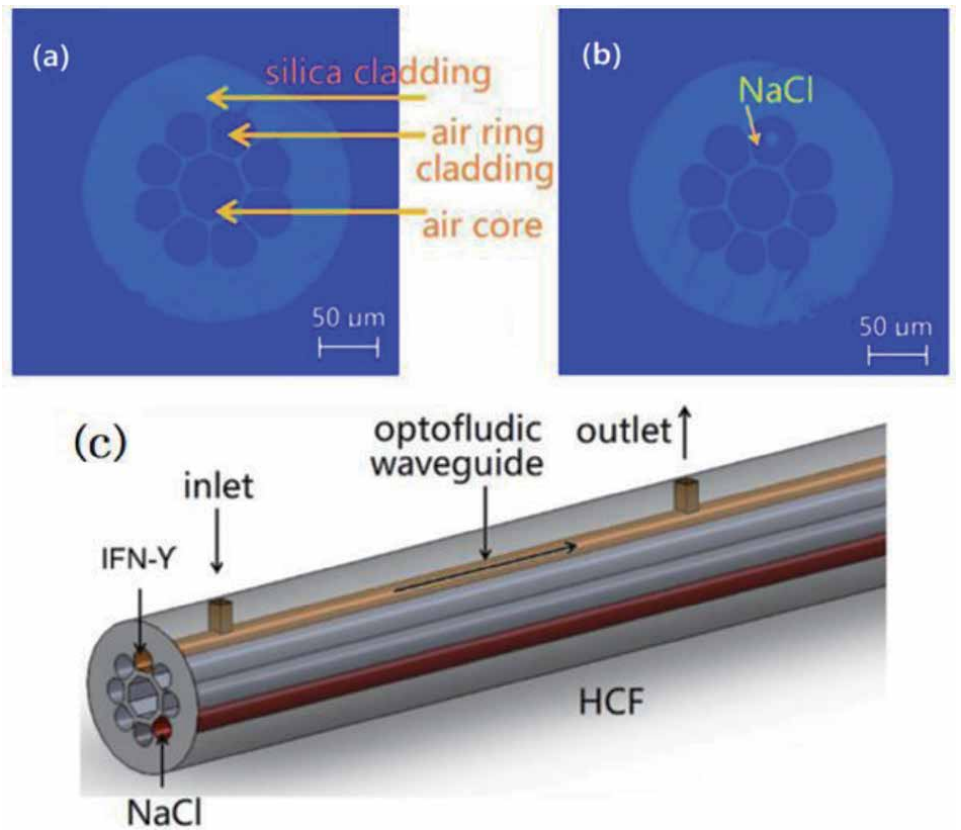

Figure 8.
(a) The cross section of the HCF. (b) The cross-section of the NaCl-infiltrated HCF. (c) The schematic diagram of the dual-optofluidic waveguide ARROW [12].

solution for ~48 h, as shown in **Figure 8(b)**. The liquid sample could be also pumped out of the hole through the other microchannel, as an outlet, as shown in **Figure 8(c)** [12].

The cross-sectional schematic diagram of the optical fiber biosensor is shown in **Figure 9(a)**, which can be described by a DL-ARROW model [12]. Due to the infiltration of IFN-γ or NaCl with high RI in the cladding of HCF, the guided light will reflect at the two interfaces of the cladding, thus forming a Fabry-Pérot resonator, as shown in **Figure 9(b)**. Therefore, an ARROW is formed in HCF. However, due to two different infiltration materials, the IFN-γ solution and the NaCl solution, two ARROWs appear in HCF. At the wavelength of 1550.38 nm, the resonance condition of the ARROW for the optofluidic waveguide is achieved [12]. On the other hand, at the wavelength of 1557.86 nm, the resonance condition of the ARROW for the NaCl-infiltrated channel is achieved [13]. Hence, there are two resonance dips corresponding to two materials, which can be expressed as Eqs. (6) and (7) [12, 13]:

$$\lambda_o = \frac{2\left(d_{op}\sqrt{n_{op}^2 - n_{air}^2} + d_{cl}\sqrt{n_{silica}^2 - n_{air}^2}\right)}{m} \tag{6}$$

$$\lambda_n = \frac{2\left(d_{op}\sqrt{n_{na}^2 - n_{air}^2} + d_{cl}\sqrt{n_{silica}^2 - n_{air}^2}\right)}{m} \tag{7}$$

where m is the resonance order, λ_o and λ_n are wavelengths of resonance dips for IFN-γ and NaCl solution, d_{op} and d_{cl} are diameters of the hole and thickness of the silica cladding, and n_{air}, n_{op}, n_{na} and n_{silica} are RIs of the core, IFN-γ solution, NaCl solution, and silica, respectively.

Due to the change of RI in the optofluidic waveguide [12], the immunoreaction between the aptamer and the IFN-γ could modulate the wavelength of the resonant dip for the IFN-γ infiltrated ARROW. However, the resonant wavelength dip is fixed because of the channel independence of NaCl-infiltrated resonator. On the other side, due to the similar thermos-optical coefficients of the NaCl and IFN-r, the wavelength shifts of two resonance dips corresponding to two ARROWs have the same response to the temperature fluctuation [12]. The response of the two resonance attenuation wavelength shifts corresponding to the two ARROWs to temperature fluctuation is the same. Therefore, a dual-optofluidic waveguide ARROW

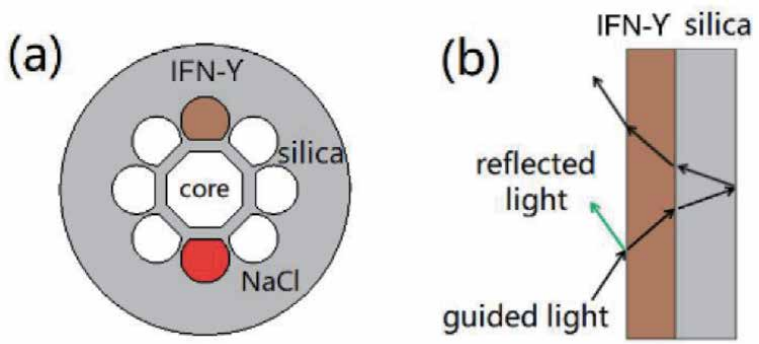

Figure 9.
(a) Diagram of the dual-optofluidic waveguide ARROW and (b) the Fabry-Pérot resonator [12].

biosensor with temperature compensation is formed by interrogating and inquiring the wavelength interval between the two resonance dips of the dual-optofluidic flow waveguide ARROW [12, 13].

The biosensor of DR-ARROW was also tested [12]. The corresponding transmission spectra, **Figure 1A** is shown in Appendix [12]. The transmission spectrum of the ethanol and NaCl infiltrated the dual-optofluidic waveguide ARROW biosensor, **Figure 1A(a)** is shown in Appendix [12]. There are two resonance dips in the wavelength range of 1525–1565 nm. The resonance dips at 1545.58 and 1550.86 nm are consistent with the theoretical predictions of the ethanol-infiltrated Fabry-Pérot cavity (1545.78 nm) and the NaCl-infiltrated Fabry-Pérot cavity (1550.38 nm) [12]. Therefore, there will be two resonance dips if the two materials infiltrated Fabry-Pérot resonators at the same time. Different concentrations of ethanol solution are injected into the optofluidic waveguide channel, and the corresponding RI changes from 1.3568 to 1.3622 RIU. When the temperature is 20° C, the wavelength shift of the ARROW of dual-optofluidic waveguide with different RIs, **Figure 1A(b)** is shown in Appendix [12]. The wavelengths of two resonance attenuations for different RIs, **Figure 1A(C)** is shown in Appendix [12]. In addition, the wavelength spacing of the two resonance dips, **Figure 1A(d)** is shown in Appendix [12]. In this experiment, if the resolution of OSA is 0.02 nm, the sensitivity of RI response can reach −1413 nm/RIU [12].

In addition, the effect of temperature on the biosensor was investigated by experiments [12]. The transmission spectra of the biosensor at different temperatures from 20 to 80°C are shown in **Figure 10(a)** [12]. At different temperatures, the two resonance decays shift to longer wavelengths at the same time. However, due to the same temperature response of the two ARROWs, the wavelength interval is maintained at a standard change of 0.02 nm, as shown in **Figure 10(b)** [12]. Hence, the dual-optofluidic waveguide ARROW biosensor is not sensitive to temperature by interrogating the wavelength interval [12].

3.4 The hybrid antiresonant reflecting optical waveguide sensor

Most of the ARROW-based fiber sensors only rely on the working principle of the ARROW. In recent years, the fiber optic sensor of the hybrid antiresonant reflecting optical waveguide (H-ARROW) has been researched. Besides the ARROW, another mechanism was also formed in the fiber, making a hybrid

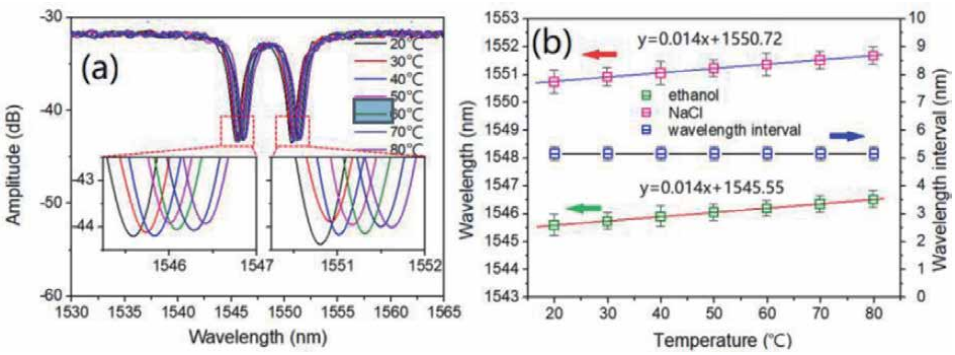

Figure 10.
(a) Wavelength shifts at different temperature from 20 to 80°C and (b) wavelength of resonance dips and the wavelength interval [12].

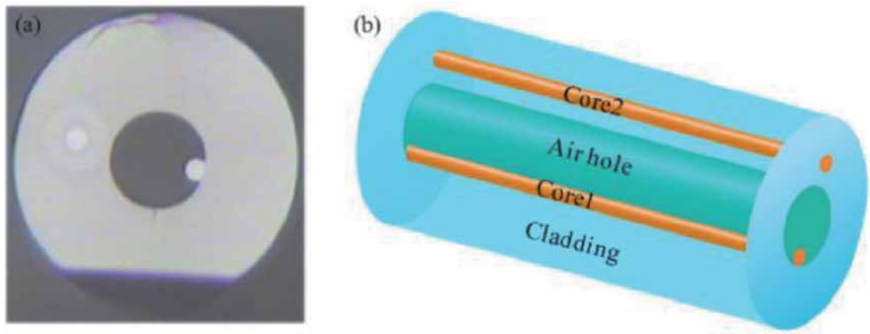

Figure 11.
(a) The cross section of single-hole twin eccentric core fiber and (b) three-dimensional diagram of single-hole twin eccentric core fiber [15].

mechanism in a single ARROW-based fiber sensor [14, 15]. The two different mechanisms could measure different parameters dependently, which increase the multifunction of the ARROW-based fiber sensor significantly. In this section, a curvature ARROW-based fiber sensor with hybrid mechanism is introduced as an example [15].

Optical fiber curvature sensors have been widely used in structural health monitoring and distributed sensing fields, such as buildings, towers, and bridges [15, 29]. The optical fiber curvature sensor has the advantages of small volume, high sensitivity, and no electromagnetic interference [30, 31]. Here, an all-fiber vibration sensor is based on H-ARROW, through the integrated antiresonance mechanism and in-line Mach Zehnder interference (MZI) [32]. The schematic construction of the proposed curvature sensor is given in **Figure 11** [15]. The single-hole double-core fiber is characterized by replacing the core with a large air hole, one of which is suspended on the inner surface of the cladding. As shown in **Figure 11(a)**, the other core is asymmetrically distributed outside the air hole. As can be seen from **Figure 11(b)**, for the curvature fiber, Core 1 is suspended in the air hole in the middle of the hollow-core fiber, and Core 2 is in the cladding of the hollow-core fiber [15].

The principle of curvature sensor of H-ARROW is analyzed [15]. According to its structure, the single-hole dual-core fiber is characterized by replacing the core with a large air hole, one of which is suspended on the inner surface of the cladding, as shown in **Figure 12** [15]. According to the working principle of the single-hole double-eccentric core fiber, the distribution of light field in the whole fiber is of great significance [15]. A section of a 2.6 mm single-hole double-eccentric core fiber is fused between two single-mode fibers. It is well known that when a beam travels between different media, it will reflect and refract. Specifically, for the beams propagating from the optical dense medium to the optical thin film medium, only when the incident angle is less than the critical incident angle, the two effects exist at the same time [15].

The transmission spectrum of the optical fiber sensor is controlled by two effects: antiresonance and in-line MZI [15]. It should be noted that the backscattered beam undergoes multiple reflections in the cladding. As a result, Fabry-Pérot resonators are formed in a silicon cladding. The antiresonance effect of the single-hole double eccentric core fiber can be regarded as the reflection type Fabry-Pérot interferometer. Therefore, the transmission of the antiresonance effect can be expressed as Eq. (8) [15, 32]:

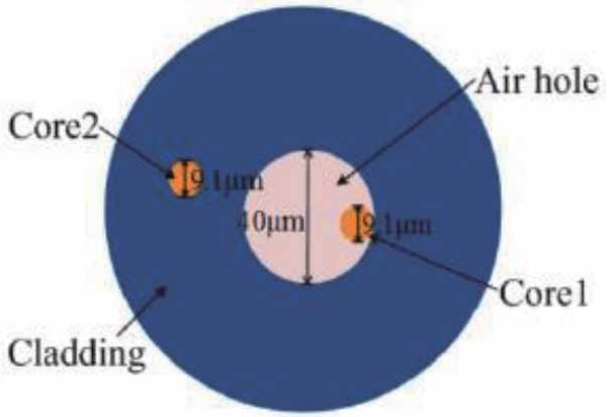

Figure 12.
The cross-sectional microscope images of the single-hole twin eccentric core fiber [15].

$$T_{anti} = A\frac{F\sin^2\left(\frac{2\pi}{\lambda}\mathrm{n}(\lambda)l\right)}{1+F\sin^2\left(\frac{2\pi}{\lambda}\mathrm{n}(\lambda)l\right)} \tag{8}$$

where F represents the fringe finesse coefficient of the multiple-beam interferometer. λ and n(λ) are the wavelengths of the spectrum and effective RI of the cladding, respectively. A and l are the intensity coefficients of the whole antiresonant effect and optical path of the antiresonant beams. In addition, the wavelength at resonance can be obtained by the following equation as Eq. (9) [15, 32]:

$$\lambda_{anti} = \frac{2d}{m}\sqrt{n_1^2 - n_2^2} \tag{9}$$

where d is the thickness of the single-hole twin eccentric core fiber cladding, and m is the resonance order. n_1 and n_2 are the RIs of the single-hole twin eccentric core fiber cladding and the air, respectively.

The sensor structure also produces MZ interference rather than the antiresonance effect. As shown in **Figures 11(a)** and **(b)**, the in-line MZ structure forms several modes, including core mode, low-order mode, and high-order cladding mode. The dominant interference is formed between the core mode and the low-order cladding mode. Therefore, the transmission of the multimode interference can be normalized as Eq. (10) [15, 32]:

$$T_{MZi} = B_i\cos^2\left(\frac{\pi}{\lambda}\cdot\Delta n_i\cdot L\right) \tag{10}$$

where B_i is the intensity coefficient of the comb spectrum, Δn_i is the effective RI difference between the fiber core mode and cladding modes, L is the physical length of the special fiber cladding, and i represents the order of the cladding modes.

A curvature experiment is conducted to investigate the sensing properties [15]. The test results are shown in **Figure 13**. The sensing characteristics are investigated by the curvature experiment [15]. The test results are shown in **Figure 13**. The curvature variation can be derived from 0.94 to 2.10 m^{-1} according to the equation of $Rsin(L/2R) = (L-d)/2$ [15]. In this experiment, fitted resonant wavelength

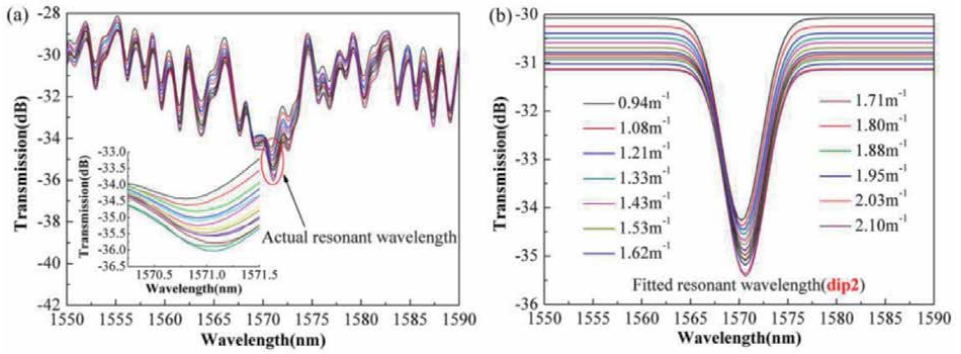

Figure 13.
(a) The intensity variation of the actual resonant wavelength with the curvature increased and (b) the intensity variation of the Gaussian fits resonant wavelength (dip2) with curvature increasing from 0.94 to 2.1 m^{-1} [15].

(dip2) is selected to monitor the curvature variation trend, corresponding to the resonant wavelength of 1570 nm [15]. The intensity of the actual wavelength decreases as the curvature increases, as shown in **Figure 13**. The intensity of the actual resonant wavelength decreases as the curvature increases, as shown in **Figure 13(a)** [15]. The actual wavelength circled by the red ellipse is about 1571 nm, and the inset is the enlarged view of the intensity variation [15]. The actual wavelength circled by the red ellipse is about 1571 nm, and the illustration is an enlarged picture of intensity change [15]. **Figure 13(b)** reflects that there is also only intensity variation without wavelength shift. The Gaussian fitting resonant wavelength of dip2 undergoes intensity decreasing when the curvature increases from 0.94 to 2.10 m^{-1} [15].

4. Conclusion

In summary, this chapter introduces the optical fiber sensors based on ARROW. According to the working principle, the optical fiber sensors based on ARROW consist of the single layer, double layers, double resonators, and hybrid mechanism. Various optical fiber sensors based on ARROW have been introduced in this chapter with the aforementioned working principle, including the fiber optic vibration sensor, humidity sensor, strain sensor, temperature sensor, magnetic field sensor, biosensor, etc. The optical fiber sensors based on ARROW could enhance the interaction between the guided light and sensitive material, simplify the complexity of the sensor configuration, and increase the multifunctional performance of the fiber sensor. Especially, many long-standing challenges in the fiber optic sensor can be solved through the working principle of the ARROW, including the temperature cross-talk compensation, distribution localization, and optofluidic biosensing. In general, the optical fiber sensors based on ARROW have advantages, such as compact structure, high sensitivity, large dynamic range, and high stability, which appear to have potential applications in researches of structure health monitoring, oil exploiting, and biology detection.

Acknowledgements

The authors acknowledge the China National Key R&D Program (No. 2019YFA0706304) and the National Natural Science Foundation of China (Nos. 61835002, 61675033, 61727817, and 61601436).

Conflict of interest

The authors declare no conflicts of interest.

Appendix

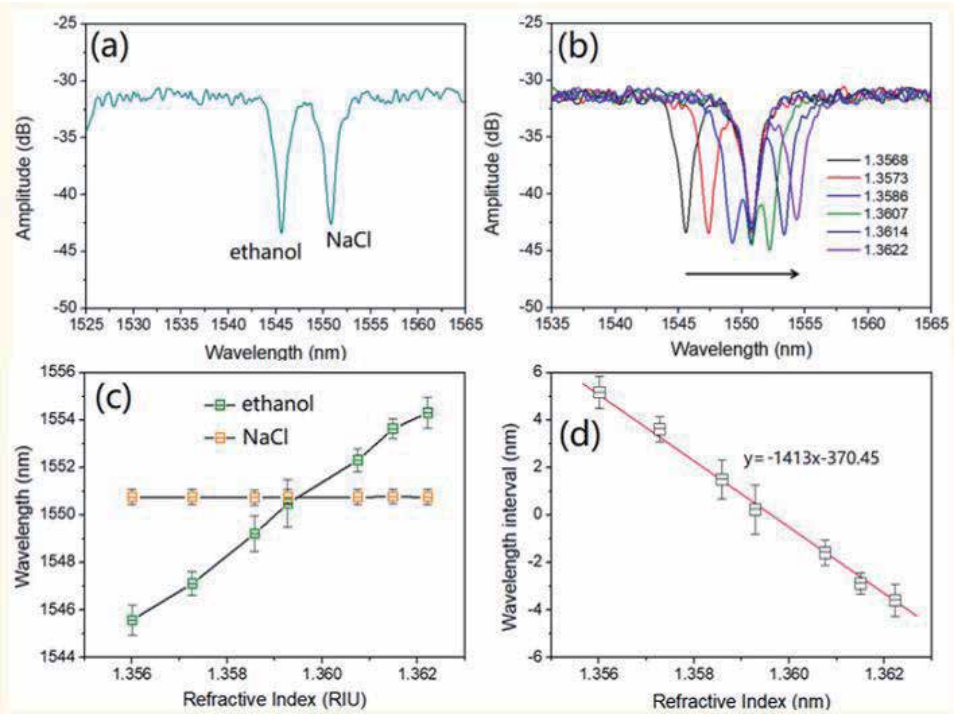

Figure 1A.
(a) Transmission spectrum of the dual-optofluidic waveguide ARROW biosensor, (b) wavelength shifts with different RI, (c) relationship between the wavelengths of resonance dips and RI, and (d) wavelength interval with different RIs [12].

Author details

Ran Gao[1*†] and Jiansen Ye[2†]

1 Advanced Research Institute of Multidisciplinary Science, Beijing Institute of Technology, Beijing, China

2 School of Information Engineering, Zhengzhou Institute of Technology, Zhengzhou, China

*Address all correspondence to: 6120190142@bit.edu.cn, forest929@163.com

† These authors are contributed equally to this work.